

# Novel Radar Waveform Optimization for a Cooperative Radar-Communications System

Alex R. Chiriyath, *Student Member, IEEE*, Shankarachary Ragi, *Member, IEEE*,  
Hans D. Mittelmann and Daniel W. Bliss, *Fellow, IEEE*

**Abstract**—We develop and present the novel *minimum estimation error variance* waveform design method, that optimizes the spectral shape of a unimodular radar waveform such that the performance of a joint radar-communications system that shares spectrum is maximized. We also develop the novel spectral water-filling SIC data rate which employs the continuous spectral water-filling algorithm to obtain the optimal communications power spectrum. We also perform a numerical study to compare the performance of the new technique with the previously derived spectral mask shaping method. The global estimation rate and the data rate capture the radar and the communications performance respectively.

**Index Terms**—Joint Radar-Communications, Radar Waveform Design, Successive Interference Cancellation, Continuous Spectral Water-Filling, Non-convex Optimization

## I. INTRODUCTION

Spectral congestion is quickly becoming a problem for the telecommunications sector [1] and cooperative spectrum sharing between radar and communications systems such that both systems mutually benefit from the presence of each other has been proposed as a potential solution [2, 3]. In order to determine how to efficiently share spectral resources and achieve RF convergence [4], a through understanding of the fundamental performance limits of cooperative spectrum sharing is needed. References [3, 5] investigated the fundamental limits of a in-band cooperative radar and communications system and developed inner bounds on performance for such a system. However, these bounds were specifically developed by considering only local estimation errors and with a radar waveform that is suboptimal for joint performance. Generalizing these performance bounds can help to establish limits for cooperative spectrum sharing.

Furthermore, these joint radar-communications performance bounds were found to depend on the shape of the radar waveform spectrum [3, 5]. For a given bandwidth, an impulse-like radar spectral shape (small root mean square (RMS) bandwidth) was found to be more favorable for communications

The work of A. R. Chiriyath and D. W. Bliss was supported in part by the Office of Naval Research. Any opinions, findings, and conclusions or recommendations expressed in this material are those of the authors and do not necessarily reflect the views of the Office of Naval Research or the U.S. Government. The work of S. Ragi and H. D. Mittelmann was supported in part by Air Force Office of Scientific Research under grant FA 9550-15-1-0351.

A.R. Chiriyath and D.W. Bliss are with the Bliss Laboratory of Information, Signals, and Systems and the Center for Wireless Information Systems and Computational Architectures (WISCA), Arizona State University, Tempe, AZ 85281 USA. S. Ragi and H. D. Mittelmann are with the School of Mathematical and Statistical Sciences, Arizona State University, Tempe, AZ 85287 USA.

performance, whereas a radar waveform spectrum with more energy at the edges of the bandwidth allocation (large RMS bandwidth) were found to be more favorable for estimation performance. However, the latter waveform also has higher autocorrelation side-lobes or ambiguity which negatively impact the global (local and non-local regime) estimation performance by increasing the radar threshold signal-to-noise ratio (SNR) at which non-local estimation errors occur. Thus, the shape of the radar spectrum poses a trade-off both in terms of radar performance vs. communications performance and in terms of improved estimation performance vs. an increased radar threshold SNR.

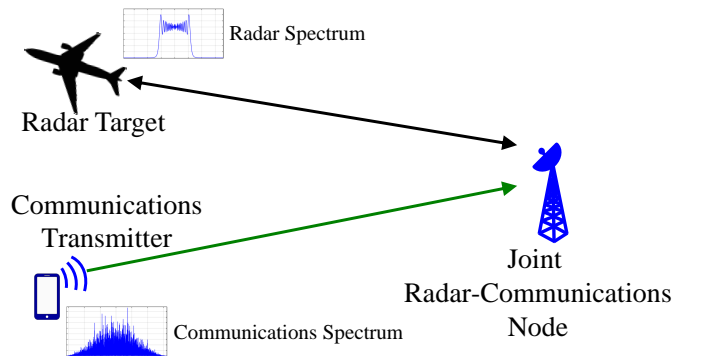


Fig. 1. The joint radar-communications system simulation scenario for radar waveform design. In this scenario, a radar and communications user attempt to use the same spectrum-space-time. This scenario is instructional, and can easily be scaled to more complicated scenarios by using it as a building block to construct real world examples.

Reference [6] generalized the performance bounds developed in References [3, 5] by taking non-local estimation errors into account and tuning the shape of the radar waveform spectrum to maximize joint radar-communications performance. The results presented in this paper is an extension of the work presented in Reference [6]. In this paper, we present a new radar waveform design method for a joint radar-communications system that optimizes the radar waveform spectrum to maximize radar performance or minimize estimation error variance in the non-local (or low-SNR) regime and optimizes the communications power spectrum to maximize communications performance by employing the continuous spectral water-filling algorithm [7]. This novel method designs a jointly optimal radar waveform that is constant modulus, unlike the method presented in Reference [6]. The global estimation rate, introduced in [6], and data rate capture radar

67 and communications performance respectively. In order to  
 68 place emphasis on waveform design approaches and their  
 69 performance, we assume a simple scenario with a single target  
 70 and no clutter. The problem scenario considered in this paper  
 71 is given by Figure 1.

### 72 A. Contributions

73 The main contributions of this paper are summarized below.

- 74 • Develop novel *minimum estimation error variance* wave-  
 75 form design method to design a constant modulus radar  
 76 waveform that maximizes radar performance of a joint  
 77 radar-communications system
- 78 • Develop novel spectral water-filling SIC data rate that  
 79 maximizes communications performance of a joint radar-  
 80 communications system
- 81 • Perform numerical study on the effects of radar threshold  
 82 SNR and the order of non-linear chirp phase on waveform  
 83 design performance
- 84 • Compare performance of new waveform design algorithm  
 85 with previously derived *spectral-mask shaping* waveform  
 86 design method

### 87 B. Background

88 The performance bounds presented in References [3–5, 8],  
 89 which only considered local estimation errors, were shown  
 90 to be dependent primarily on the RMS bandwidth of the  
 91 radar waveform. Reference [6] extended the estimation rate to  
 92 consider non-local or global estimation errors and employed  
 93 a spectral mask to shape the radar waveform spectrum so as  
 94 to maximize the performance of a joint radar-communications  
 95 system. An evolutionary optimization algorithm was applied  
 96 to find the optimal spectral mask that maximizes radar and  
 97 communications performance (estimation and data rate re-  
 98 spectively) and new performance bounds were developed.  
 99 Performance bounds comparing communications performance  
 100 versus radar detection performance were derived for a joint  
 101 radar-communications system in Reference [9].

102 Modern approaches to the RF convergence problem have  
 103 looked at waveform design in the context of a single, uni-  
 104 fied waveform for radar and communications. For exam-  
 105 ple, orthogonal frequency-division multiplexing (OFDM) is  
 106 commonly chosen for this dual waveform [10–14], where a  
 107 single transmission is used for communications and monostatic  
 108 radar. Most results using OFDM waveforms revealed data-  
 109 dependent ambiguities, opposing cyclic prefix requirements,  
 110 and demanding peak-to-average power ratio (PAPR) require-  
 111 ments. Spread spectrum waveforms have also been proposed  
 112 for their autocorrelation properties [15–17], and MIMO radar  
 113 techniques have been suggested, given that the independent  
 114 transmitted waveforms allow more degrees of freedom for  
 115 joint radar-communications co-design [18–20]. Multiple or-  
 116 thogonal linear frequency modulated chirps have also been  
 117 proposed to accomplish both radar detection and communica-  
 118 tions transmissions in a MIMO system [21]. Both systems have  
 119 fundamentally different waveform requirements and that is  
 120 why, contrary to the aforementioned approaches, the waveform

design method proposed in this paper assumes that radar and  
 communications systems transmit separate waveforms.

121 Researchers have also looked at optimization theory based  
 122 radar waveform design methods that look to optimize radar  
 123 performance while the communications system is constrained  
 124 to reduce interference. Optimization theory is used to maxi-  
 125 mize some radar performance metrics (detection probability,  
 126 ambiguity function features etc.) and keep interference to other  
 127 in-band systems at a minimum [22–24] or impose constraints  
 128 on the communications rate of other in-band systems [25].

129 Researchers have searched several other research areas for  
 130 potential solutions to the spectral congestion problem. Some  
 131 researchers looked at spatial mitigation as a means to improve  
 132 spectral interoperability [26–28]. Joint coding techniques, such  
 133 as robust codes for communications that have desirable radar  
 134 ambiguity properties, as well as codes that trade data rate and  
 135 channel estimation error have been investigated as co-design  
 136 solutions [29–32].

### 137 C. Problem Set-up

138 We consider the scenario shown in Figure 1, which in-  
 139 volves a radar and communications user attempting to use  
 140 the same spectrum-space-time. We consider the joint radar-  
 141 communications receiver to be a radar transmitter/receiver that  
 142 can act as a communications receiver. The key assumptions  
 143 made in this paper for the scenario described in Figure 1 are  
 144 as follows

- 145 • Joint radar-communications receiver is capable of simul-  
 146 taneously decoding a communications signal and estimat-  
 147 ing a target parameter
- 148 • Radar detection and track acquisition have already taken  
 149 place
- 150 • Radar system is an active, single-input single-output  
 151 (SISO), mono-static, and pulsed system
- 152 • Inter-pulse ambiguities between radar pulses not consid-  
 153 ered
- 154 • A single SISO communications transmitter is present
- 155 • Only one radar target is present
- 156 • Target range or delay is the only parameter of interest
- 157 • Target cross-section is well estimated

158 It should be noted that the performance bounds and results  
 159 presented in this paper are very closely dependent on the em-  
 160 ployed receiver model. By employing a mitigation technique  
 161 called successive interference cancellation (SIC) (discussed  
 162 later in the paper) at the receiver, the communications data  
 163 rate at the receiver becomes dependent on the radar waveform  
 164 spectrum [5]. Employing different mitigation techniques and  
 165 changing the receiver model will result in a set of performance  
 166 bounds that are different from the ones presented in this paper.

## 167 II. THE JOINT RADAR-COMMUNICATIONS SYSTEM - 168 RECEIVER MODEL AND PERFORMANCE METRICS

169 In this section, we present both the model used to represent  
 170 the joint radar-communications receiver and the performance  
 171 metrics used in this paper to characterize radar and com-  
 172 munications performance for the joint radar-communications

175 system. A discussion of the SIC mitigation techniques em-  
 176 ployed at the receiver is also provided. We present a table of  
 177 significant notation that is employed in this paper in Table I.

TABLE I  
 SURVEY OF NOTATION

Variable	Description
$\langle \cdot \rangle$	Expectation
$\  \cdot \ $	L2-norm or absolute value
$Q_M(\cdot)$	Marcum Q-function
$\delta(\cdot)$	Dirac-delta function
$f$	Frequency
$t$	Time
$B$	Full bandwidth of the system
$B_{\text{rms}}$	Root-mean-squared radar bandwidth
$x(t)$	Unit-variance transmitted radar signal
$X(f)$	Radar signal frequency response
$P_{\text{rad}}$	Radar power
$\tau$	Time delay to target
$a$	Target complex combined antenna, cross-section, and propagation gain
$T$	Radar pulse duration
$\delta$	Radar duty factor
$P_{\text{com}}$	Total communications power
$b$	Complex combined antenna gain and communications propagation loss
$n(t)$	Receiver thermal noise
$n_{\text{resi}}(t)$	Post-SIC radar residual
$\sigma_{\text{noise}}^2$	Thermal noise power
$k_B$	Boltzmann constant
$T_{\text{temp}}$	Absolute temperature
$\sigma_{\tau, \text{proc}}^2$	Variance of range fluctuation process
$\sigma_{\text{CRLB}}^2$	Cramèr-Rao lower bound or estimation error variance
ISNR	Integrated radar SNR
$p_1, \dots, p_N$	Phase parameters of polynomial chirp

### 178 A. Successive Interference Cancellation Receiver Model

179 We present the joint radar-communications receiver model  
 180 that employs SIC, an interference mitigation technique. It is  
 181 this receiver model that causes communications performance  
 182 to be closely tied to the spectrum of the radar waveform. This  
 183 receiver model was first developed in Reference [3].

184 We assume we have some knowledge of the radar target  
 185 range (or time-delay), based on prior observations, up to  
 186 some random fluctuation or process noise which is mod-  
 187 eled as a zero-mean random variable  $n_{\tau, \text{proc}}(t)$ . Using this  
 188 information, we can generate a predicted radar return and  
 189 subtract it from the joint radar-communications received sig-  
 190 nal. Since there is some error in the predicted and actual  
 191 target locations, this predicted radar signal suppression leaves  
 192 behind a residual contribution,  $n_{\text{resi}}(t)$ , to the joint received  
 193 signal. By lowering the communications rate, the receiver  
 194 can perfectly decode the communications message from the  
 195 radar-suppressed joint received signal (which consists of the  
 196 communications signal, thermal noise and radar residual).  
 197 The joint radar-communications receiver uses the decoded  
 198 communications message to reconstruct and remove the com-  
 199 munications waveform from the received signal to obtain a  
 200 radar return signal free of communications interference. This  
 201 method of interference cancellation is called SIC. SIC is the  
 202 same optimal multiuser detection technique used for a two user  
 203 multiple-access communications channel [7, 33], except it is  
 204 now reformulated for a communications and radar user instead  
 205 of two communications users. The block diagram of the joint

206 radar-communications system considered in this scenario is  
 207 shown in Figure 2. For a joint radar-communications received

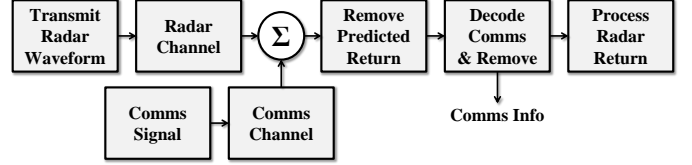


Fig. 2. Joint radar-communications system block diagram for SIC scenario. The radar and communications signals have two effective channels, but arrive converged at the joint receiver. The radar signal is predicted and removed, allowing a reduced rate communications user to operate. Assuming near perfect decoding of the communications user, the ideal signal can be reconstructed and subtracted from the original waveform, allowing for unimpeded radar access.

207 signal,  $z(t)$ , given by

$$z(t) = b\sqrt{P_{\text{com}}}r(t) + n(t) + \sqrt{P_{\text{rad}}}ax(t-\tau),$$

208 the received signal at the communications receiver with the  
 predicted radar return suppressed,  $\tilde{z}(t)$ , is given by [3, 5]

$$\tilde{z}(t) = b\sqrt{P_{\text{com}}}r(t) + n(t) + \sqrt{P_{\text{rad}}}a[x(t-\tau) - x(t-\tau_{\text{pre}})],$$

where  $x(t-\tau_{\text{pre}})$  is the predicted radar return signal, and  $\tau_{\text{pre}}$  is the predicted target delay. When applying SIC, the interference residual plus noise signal  $n_{\text{int}+n}(t)$ , from the communications receiver's perspective, is given by [3, 5]

$$n_{\text{int}+n}(t) = n(t) + n_{\text{resi}}(t) = n(t) + \sqrt{\|a\|^2 P_{\text{rad}}} n_{\tau, \text{proc}}(t) \frac{\partial x(t-\tau)}{\partial t},$$

209 where  $n_{\tau, \text{proc}}(t)$  is the process noise with variance  $\sigma_{\tau, \text{proc}}^2$ .

210 It should be noted that SIC performance is highly sensitive  
 211 to model mismatch errors since they introduce larger residuals  
 212 in the SIC process, negatively impacting interference cancel-  
 213 lation performance. Potential sources for model mismatch in-  
 214 clude dynamic range constraints on the receiver or transmitter,  
 215 phase noise etc. Insufficient transmitter or receiver dynamic  
 216 range implies that if one received signal is stronger than the  
 217 other signal, mitigating the stronger signal through SIC will  
 218 be incredibly difficult, resulting in high residual values being  
 219 present in the weaker signal after SIC. Communications signal  
 220 mitigation by 40-50 dB has been demonstrated experimen-  
 221 tally [34, 35]. As a result, a dynamic range of 50 dB is  
 222 sufficient to avoid model mismatch errors for the joint radar-  
 223 communications receiver. Additionally, it should be noted that  
 224 the performance of the SIC receiver has a complex dependency  
 225 on receiver phase noise. Large phase noise can introduce larger  
 226 post-radar suppression residual values, negatively impacting  
 227 joint radar-communications performance. A better analysis of  
 228 the relationship between the SIC receiver and phase noise can  
 229 be found in [36].

### 230 B. Spectral Water-filling SIC Data Rate

231 We develop and present the novel spectral water-filling SIC  
 232 data rate, which utilizes the continuous spectral water-filling

algorithm [7, 37] to determine the optimal communications power distribution over frequency. The continuous spectral water-filling algorithm optimizes the data rate for a given noise power spectral density [7, 37]. Once the receiver model is known, the communications transmitter can easily determine the noise spectral density at the receiver,  $N_{\text{int+n}}(f)$ , and apply the continuous spectral water-filling algorithm to determine the optimal communications transmit power distribution,  $P(f)$ . This communications power distribution,  $P(f)$ , maximizes the communications data rate at which the joint radar-communications receiver decodes the communications message. We define this maximized communications rate as the spectral water-filling SIC data rate. The spectral water-filling SIC data rate is the data rate that will be used to measure communications performance. The continuous spectral water-filling algorithm is a continuous form extension of the water-filling algorithm employed in References [3, 5]. Figure 3 highlights how the continuous spectral water-filling algorithm selects the optimal power distribution.

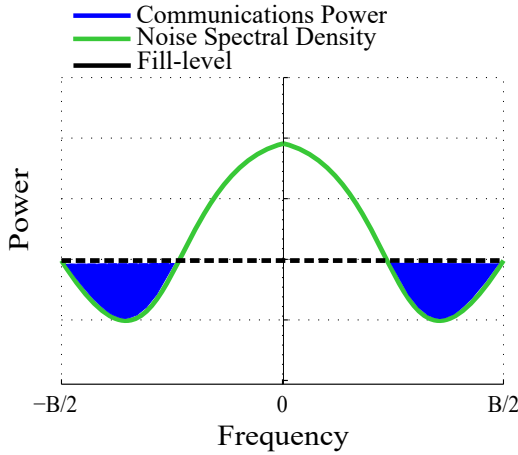


Fig. 3. A notional example of the continuous spectral water-filling algorithm. The black, dashed line indicates the fill level (maximum amount of communications power that can be allocated at any frequency), the green curve represents the noise power spectral density  $N_{\text{int+n}}(f)$ , and the optimal communications power spectral distribution is shown in blue.

As mentioned earlier, since we employ the SIC model at the joint radar-communications receiver, the receiver will decode the communications message after the predicted radar signal has been mitigated from the received signal. As a result, from the communications receiver's perspective, the channel will be corrupted by noise given by Equation (2). In order to find the noise spectral density,  $N_{\text{int+n}}(f)$ , we first calculate the autocorrelation function of the time- and band-limited noise signal,  $n(t)$  (since the received signal is also time- and band-

limited),

$$\begin{aligned} \gamma(\alpha) &= \langle n_{\text{int+n}}(t) n_{\text{int+n}}^*(t - \alpha) \rangle \\ &= \langle n(t) n^*(t - \alpha) \rangle + \langle n_{\text{resi}}(t) n_{\text{resi}}^*(t - \alpha) \rangle \\ &= k_B T_{\text{temp}} B \text{sinc}(\pi B \alpha) \\ &\quad + \|a\|^2 P_{\text{rad}} \sigma_{\tau, \text{proc}}^2 \frac{\partial x(t - \tau)}{\partial t} \frac{\partial x^*(t - \tau - \alpha)}{\partial t} \\ &= k_B T_{\text{temp}} B \text{sinc}(\pi B \alpha) + (4\pi^2) \|a\|^2 P_{\text{rad}} \sigma_{\tau, \text{proc}}^2 \\ &\quad \cdot \int_{-\infty}^{\infty} df f^2 X(f) X^*(f) e^{i2\pi f \alpha} \\ &= k_B T_{\text{temp}} B \text{sinc}(\pi B \alpha) + (4\pi^2) \|a\|^2 P_{\text{rad}} \sigma_{\tau, \text{proc}}^2 g(\alpha), \end{aligned} \quad (3)$$

where Parseval's theorem and the time-shift and time derivative properties of the Fourier transform are used between the second and third steps,  $\text{sinc}(x) = \frac{\sin(x)}{x}$ , and  $g(\alpha)$  is the inverse Fourier transform with respect to  $\alpha$  of  $G(f) = \|X(f)\|^2 f^2$ . Since the noise power spectral density and autocorrelation are Fourier transform pairs, the noise power spectral density is given by

$$\begin{aligned} N_{\text{int+n}}(f) &= N(f) + N_{\text{resi}}(f) \\ &= k_B T_{\text{temp}} \Pi_B(f) \\ &\quad + (4\pi^2) \|a\|^2 P_{\text{rad}} \sigma_{\tau, \text{proc}}^2 \|X(f)\|^2 f^2, \end{aligned} \quad (4)$$

where  $N(f)$  and  $N_{\text{resi}}(f)$  are the Fourier transforms of  $n(t)$  and  $n_{\text{resi}}(t)$  respectively, and  $\Pi_B(f)$  is a top-hat or rectangular function from  $-\frac{B}{2}$  to  $\frac{B}{2}$ . The optimal communications power spectrum determined by the continuous spectral water-filling algorithm is given by

$$P(f) = \left( \mu - \frac{N_{\text{int+n}}(f)}{b^2} \right)^+, \quad (5)$$

where  $(x)^+ = x$  if  $x \geq 0$ ; otherwise  $(x)^+ = 0$  and  $\mu$  is a constant that is determined from the power constraint

$$P_{\text{com}} = \int_{-\frac{B}{2}}^{\frac{B}{2}} df P(f) = \int_{-\frac{B}{2}}^{\frac{B}{2}} df \left( \mu - \frac{N_{\text{int+n}}(f)}{b^2} \right)^+. \quad (6)$$

The spectral water-filling SIC data rate (the corresponding data rate for the channel with noise spectral density  $N_{\text{int+n}}(f)$ ) is given by [7, 37]

$$R_{\text{com}} = \int_{-\frac{B}{2}}^{\frac{B}{2}} df \log \left( 1 + \frac{b^2 P(f)}{N_{\text{int+n}}(f)} \right). \quad (7)$$

It should be noted that due to the complexity involved in determining analytical solutions for the integrals shown in Equations (6) and (7), these integrals are evaluated numerically to determine the optimal value for  $\mu$  and the communications data rate.

### C. Global Estimation Rate

Here, we provide a brief discussion of the global estimation rate which was first developed in Reference [6]. We measure radar performance by the estimation rate [3, 5] which measures

271 the amount of information contained in radar returns. The  
272 estimation rate is upper bounded as follows:

$$R_{\text{est}} \leq \frac{\delta}{2T} \log_2 \left[ 1 + \frac{\sigma_{\tau, \text{proc}}^2}{\sigma_{\text{est}}^2} \right], \quad (8)$$

273 where  $\sigma_{\text{est}}^2$  is the range estimation noise variance, which is  
274 bounded locally by the Cramér-Rao lower bound (CRLB)  
275 [38]. The estimation rate was extended in Reference [6] to  
276 account for global estimation errors. The method of interval  
277 errors [33, 39, 40] is employed to calculate the effect of non-  
278 local errors on time-delay estimation performance. A closed-  
279 form solution of the probability of side-lobe confusion,  $P_{s.l.}$  is  
280 obtained in terms of the values and locations of the side-lobe  
281 peaks, integrated radar SNR, and the Marcum Q-function  $Q_M$   
282 [33]. The method of intervals time-delay estimation variance  
283 is then given by

$$\sigma_{\text{est}}^2 = [1 - P_{s.l.}(\text{ISNR})] \sigma_{\text{CRLB}}^2(\text{ISNR}) + P_{s.l.}(\text{ISNR}) \phi_{s.l.}^2, \quad (9)$$

284 where  $\phi_{s.l.}$  is the offset in time (seconds) between the auto-  
285 correlation peak side-lobe and main-lobe [5]. The probability  
286 of side-lobe confusion,  $P_{s.l.}$ , is given by [33]

$$\begin{aligned} P_{s.l.}(\text{ISNR}) = 1 - Q_M \left( \sqrt{\frac{\text{ISNR}}{2}} \left( 1 + \sqrt{1 - \|\rho\|^2} \right), \right. \\ \left. \sqrt{\frac{\text{ISNR}}{2}} \left( 1 - \sqrt{1 - \|\rho\|^2} \right) \right) \\ + Q_M \left( \sqrt{\frac{\text{ISNR}}{2}} \left( 1 - \sqrt{1 - \|\rho\|^2} \right), \right. \\ \left. \sqrt{\frac{\text{ISNR}}{2}} \left( 1 + \sqrt{1 - \|\rho\|^2} \right) \right), \quad (10) \end{aligned}$$

287 where  $\rho$  is the ratio of the main-lobe to the peak side-lobe  
288 of the autocorrelation function. For a radar system performing  
289 time-delay estimation, the CRLB for time delay estimation is  
290 given by [41]

$$\sigma_{\text{CRLB}}^2 = (8\pi^2 B_{\text{rms}}^2 \text{ISNR})^{-1}, \quad (11)$$

291 where the RMS bandwidth is given by

$$B_{\text{rms}}^2 = \frac{\int f^2 \|X(f)\|^2 df}{\int \|X(f)\|^2 df}. \quad (12)$$

292 A more intuitive understanding of how the estimation rate  
293 metric captures target parameter estimation performance and  
294 the implications of altering the estimation rate can be found  
295 in [4]. The estimation rate is extended to account for Doppler  
296 measurement and continuous signaling radars in Reference  
297 [42].

### 298 III. NON-LINEAR CHIRP WITH PARAMETRIC POLYNOMIAL 299 PHASE

300 In this section, we briefly introduce the novel parameterized  
301 non-linear chirp that will be used to design the optimal radar  
302 waveform in the minimum estimation error variance waveform  
303 design method. We also derive an approximate closed-form

304 solution for the spectrum for a special case of this non-linear  
305 chirp waveform.

306 One desirable property for radar waveforms is to have a  
307 peak-to-average power ratio as close as possible to 1 (the  
308 smallest possible value). Thus, most radar systems now require  
309 the signal to be constant modulus or unimodular, which  
310 keeps the peak and the average power the same over any  
311 time period, granting the signal the smallest possible peak-to-  
312 average power ratio of 1. To ensure that the optimized radar  
313 waveform is unimodular, we begin by considering the fol-  
314 lowing unimodular non-linear chirp signal with a polynomial  
315 phase

$$x(t) = e^{i\pi(\sum_{m=1}^N p_m t^{2m})}, \quad (13)$$

316 where  $N$  is a positive integer and  $p_m \in \mathbb{R}, \forall m$  are phase coef-  
317 ficients. We let the polynomial phase to have only even terms  
318 to ensure symmetry in the frequency domain. The shape of the  
319 waveform spectrum is determined by the phase coefficients.  
320 The minimum estimation error variance method selects the  
321 appropriate phase coefficient values so as to optimize the shape  
322 of the radar spectrum to maximize joint radar-communications  
323 performance.

324 In the following discussion, we derive an approximate  
325 expression for the spectrum of the non-linear chirp waveform  
326 shown in Equation (13) for the case that  $N = 2$ .

#### 327 A. Spectrum of Non-linear Chirp with Parametric Polynomial 328 Phase

Due to the increased complexity involved in evaluating the  
spectrum for higher values of  $N$ , we consider the simple case  
of  $N = 2$ . The spectrum of the band-limited non-linear chirp  
with bandwidth  $B$  and time-duration  $T$  is given by

$$\begin{aligned} X(f) &= \int_{-\frac{T}{2}}^{\frac{T}{2}} dt e^{i\pi(p_1 B^2 t^2 + p_2 B^4 t^4)} e^{-i2\pi f t} \\ &= \int_{-\frac{T}{2}}^{\frac{T}{2}} dt e^{i\pi(p_1 B^2 t^2 + p_2 B^4 t^4 - 2ft)} \\ &= \int_{-\frac{T}{2}}^{\frac{T}{2}} dt e^{i\phi(t,f)}. \quad (14) \end{aligned}$$

In order to obtain a closed form solution for the above integral,  
we employ the principle of stationary phase [43]. We first find  
the points in time,  $t_0$ , where the phase,  $\phi(t, f)$ , is stationary  
i.e. when

$$\begin{aligned} \frac{\partial \phi(t, f)}{\partial t} \Big|_{t=t_0} &= 0 \\ \Rightarrow \pi(2p_1 B^2 t_0 + 4p_2 B^4 t_0^3 - 2f) &= 0 \\ \Rightarrow 2p_1 B^2 t_0 + 4p_2 B^4 t_0^3 - 2f &= 0 \end{aligned} \quad (15)$$

Solving for  $t_0$ , we get

$$\begin{aligned} t_0 &= \frac{-6^{\frac{2}{3}} B^6 p_1 p_2}{Q} \\ &+ \frac{6^{\frac{1}{3}} (9 B^8 p_2^2 f + \sqrt{3 B^{16} p_2^3 (2 B^2 p_1^3 + 27 p_2 f^2)})^{\frac{2}{3}}}{Q} \end{aligned} \quad (16)$$

where

$$Q = 6 B^4 p_2 (9 B^8 p_2^2 f + \sqrt{3 B^{16} p_2^3 (2 B^2 p_1^3 + 27 p_2 f^2)})^{\frac{1}{3}}.$$

Using the principle of stationary phase, the expression for an approximation of the spectrum is given by [43]

$$\begin{aligned} X(f) &\approx 2 \sqrt{\frac{-\pi}{2 \phi''(t_0, f)}} e^{-i \frac{\pi}{4}} x(t_0) e^{i \phi(t_0, f)} \\ &= 2 \sqrt{\frac{-1}{4 p_1 B^2 + 24 p_2 B^4 t_0^2}} e^{-i \frac{\pi}{4}} e^{i \pi (p_1 B^2 t_0^2 + p_2 B^4 t_0^4)} \\ &\quad \cdot e^{i \pi (p_1 B^2 t_0^2 + p_2 B^4 t_0^4 - 2 f t_0)} \end{aligned} \quad (17)$$

where  $\phi''(t, f) = \frac{\partial^2 \phi(t, f)}{\partial t^2} = \pi(2 p_1 B^2 + 12 p_2 B^4 t^2)$ . Although we do not use the above-discussed expression for the radar spectrum in our numerical study, nevertheless, the above result may be useful in other studies.

#### IV. RADAR WAVEFORM DESIGN METHODS

In this section, we present the two radar waveform design algorithms discussed in this paper. We first briefly discuss the spectral mask shaping method that was first introduced in Reference [6]. A novel radar waveform design method, the minimum estimation error variance method, is also presented in this section. The spectral mask shaping method will be used as a baseline to compare the performance of the minimum estimation error variance method presented in this paper.

##### A. Spectral Mask Shaping Method

We present the radar waveform design method presented in Reference [6]. This method will be used as a performance baseline to compare the performance of the novel radar waveform design method presented in this paper. The radar waveform can be designed to maximize radar estimation rate, communications rate, or some weighting therein. Without consideration of global error, waveform design can be simplified to tuning  $B_{\text{rms}}$  [3]. A closed-form, parameterized spectral mask is used to tune  $B_{\text{rms}}$  to jointly maximize both the radar and communications users' information rate.

We assume we have a linear frequency-modulated (FM) chirp which spans from  $-B/2$  to  $B/2$  in time  $T$ . We then apply a frequency domain spectral mask weighting to the chirp,  $W(f) = x + z f^2$ ,  $|f| \leq \frac{B}{2}$ . The RMS bandwidth of the resulting weighted chirp is found by assuming the chirp spectrum is approximately flat using the principle of stationary phase (PSP) [43]. As a result, the RMS bandwidth is easily calculable in closed-form for the polynomial [6]:

$$B_{\text{rms}} = \sqrt{\frac{\frac{x^2 B^3}{12} + \frac{x z B^5}{40} + \frac{z^2 B^7}{448}}{x^2 B + \frac{x z B^3}{6} + \frac{z^2 B^5}{80}}}. \quad (18)$$

Using differential evolution (DE) [44] to tune  $B_{\text{rms}}$ , the following objective function (or cost function) is optimized to maximize joint performance (radar and communications users' information rate)

$$R_{\text{total}} = R_{\text{est}}(B_{\text{rms}})^\alpha \tilde{R}_{\text{com}}(B_{\text{rms}})^{(1-\alpha)}, \quad (19)$$

where  $\tilde{R}_{\text{com}}(B_{\text{rms}})$  is the SIC communications data rate defined in Reference [3] (not to be confused with the spectral water-filling SIC data rate defined in this paper) and  $\alpha$  is a blending parameter that is varied from 0 to 1. When  $\alpha = 0$ , only communications rate is considered. When  $\alpha = 1$ , only the radar estimation rate is considered. In between, the product is jointly maximized. Note that for  $\alpha = 0.5$ ,  $R_{\text{total}}$  represents the geometric mean of the two rates. This provides a more numerically stable error term, even when  $\tilde{R}_{\text{com}} \gg R_{\text{est}}$ .

##### B. Minimum Estimation Error Variance Method

The waveform design algorithm that we propose in this section designs an optimal non-linear chirp radar waveform (as modeled in Section III) from a global estimation rate perspective. In other words, we first design the waveform to minimize the global estimation error variance (estimation error variance taking into account both non-local and local estimation errors), given by Equation (9). This minimization of the global estimation error variance is accomplished by minimizing the estimation error variance at the radar threshold SNR of the radar estimator. The threshold point of an estimator is the estimator (or radar) SNR value at which the estimator's performance deviates from the CRLB [38] due to error contributions from non-local estimation errors. At SNR values lower than the threshold point, due to autocorrelation main-lobe - side-lobe confusion, non-local estimation errors begin to contribute to estimator's error variance which causes the estimation performance to degrade and deviate from the CRLB [33]. Since the threshold point is the SNR point at which an estimator's performance deviates from the CRLB and also the SNR point at which non-local estimation errors contribute to estimation performance, minimizing the CRLB at the threshold point gives the lowest possible global estimation error variance or highest possible global estimation rate.

For a given SNR, we have to design a radar waveform that has a threshold point at that SNR and has the best (or smallest) estimation error variance. We first eliminate all radar waveforms that have a threshold point higher than the current SNR and then, from the remaining feasible solution set, we find the radar waveform that minimizes the CRLB given by Equation (11). We perform the first elimination step by imposing the following constraint on the ratio of the global estimation error variance (given by Equation (9)) and the CRLB (given by Equation (11))

$$\frac{\sigma_{\text{est}}^2}{\sigma_{\text{CRLB}}^2} \leq \delta_{\text{constraint}}, \quad (20)$$

where  $\delta_{\text{constraint}}$  is a parameter whose value determines the size of the feasible solution set. We discuss how to tune this parameter in Section V. By ensuring the above ratio stays below  $\delta_{\text{constraint}}$ , any radar waveforms with higher threshold points (SNR values) are eliminated. Figure 4 depicts how this constraint works on eliminating radar waveforms with higher threshold points.

We also introduce an additional constraint on spectral leakage (constraint  $\mathcal{C}_2$ ) to the waveform optimization problem in order to obtain optimal radar waveforms that not only



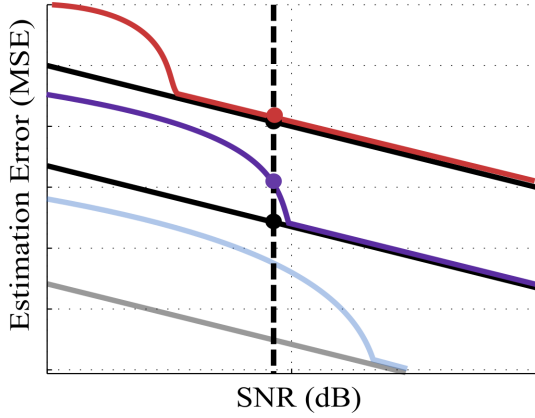


Fig. 4. A notional example depicting the impact of the constraint given by Equation (20) on the feasible set for optimization. The dashed vertical line indicates the given SNR. The red, purple and blue solid curves indicate the estimator performance for different radar waveforms and the black solid lines indicate the CRLB for each radar waveform. The black dots indicate the CRLB values for various feasible radar waveforms at the given SNR. The red and purple dots indicate the actual estimation error variance (estimation performance) for various feasible radar waveforms at the given SNR. The grayed out curves indicate estimation performance for unfeasible radar waveforms at the given SNR. Minimizing the CRLB over the feasible set ensures that the optimal radar waveform will have the lowest estimation threshold point (or best estimation performance, taking both local and non-local estimation errors).

419 ensure optimal joint radar-communications performance, but  
 420 also satisfy additional real-world properties that a traditional  
 421 radar waveform would. Since the system can only receive  
 422 signals whose spectrum lies within the system's bandwidth,  
 423 any electromagnetic radio frequency (RF) energy that leaks  
 424 outside of the bandwidth will be lost. To minimize this loss of  
 425 RF energy, we introduce a constraint on the amount of energy  
 426 present in the radar spectrum at frequencies out of the system  
 427 bandwidth range. We enforce this spectral leakage constraint  
 428 by having the radar spectrum be below a thresholding spectral  
 429 mask such as the one seen in Figure 5.

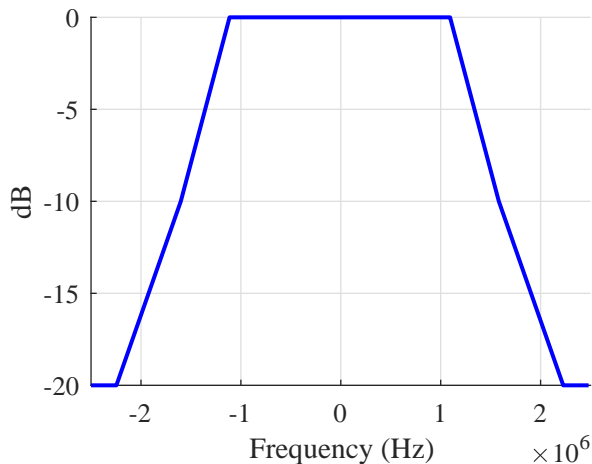


Fig. 5. Spectral Leakage Mask used constrain the amount of energy in the radar spectrum leaking out at frequencies out of the system bandwidth range. The spectral leakage constraint is enforced by having the radar spectrum be below this thresholding spectral leakage mask.

We consider the non-linear chirp waveform given by Equation (13). The spectral shape of the waveform is determined by the parameters  $p_m, m = 1, \dots, N$ . In order to design the radar waveform spectrum that minimizes the global estimation performance, we solve the following optimization problem:

$$\begin{aligned} & \underset{\bar{p}}{\text{minimize}} && \frac{1}{8\pi^2 B_{\text{rms}}(\bar{p})^2 T B(\text{SNR})}, \\ & \text{subject to} && p_m \in [0, 10] \quad \forall m \\ & && \frac{\sigma_{\text{est}}^2}{\sigma_{\text{CRLB}}^2} \leq \delta_{\text{constraint}} \\ & && \mathbb{1}_A(\bar{p}) = 1 \quad (\mathcal{C}_2) \end{aligned} \quad (21)$$

where  $\bar{p} = (p_1, \dots, p_N)$ , and  $p_1, \dots, p_N$  are the coefficients of the polynomial phase for the unimodular waveform in Equation (13), and  $B_{\text{rms}}(\bar{p})$  is given by Equation (12). The constraint  $\mathcal{C}_2$  constrains the coefficients  $\bar{p}$  such that the resulting spectrum of the waveform stays below a certain masking threshold, which is represented by an indicator function, where  $A$  is the set of all phase coefficients that let the resulting masked spectrum stay below the masking threshold as shown in Figure 5.

Once the optimal radar waveform that maximizes the radar performance of a joint radar-communications system is designed, the continuous spectral water-filling algorithm described in Section II-B is employed to determine the spectral water-filling SIC data rate that maximizes the communications performance of a joint radar-communications system. This optimization process is called the minimum estimation error variance method. It should be noted that the optimization problem described in Equation (21) is a non-convex optimization problem.

### C. Impact of Threshold Point SNR

As mentioned in Section I, we saw from References [3, 5] that the spectral shape of the radar waveform (the radar RMS bandwidth) impacts the the performance of a joint radar-communications system. Shaping the radar spectrum imposes a trade-off both in terms of radar performance vs. communications performance and in terms of improved estimation performance vs. an increased radar threshold SNR. In this subsection, we briefly discuss how the choice of the threshold SNR impacts both the shape of the radar waveform spectrum and the performance of the joint radar-communications system.

Selecting a low value for the threshold SNR implies that even for small radar SNR values, the probability of side-lobe confusion for the radar waveform autocorrelation function (which causes the estimator performance to deviate from the CRLB) is small. Radar waveforms with more energy at frequencies closer to center of the bandwidth allocation can have such autocorrelation functions. However, such a radar waveform has a smaller RMS bandwidth which degrades the overall estimation performance as seen in Equation (11). Furthermore, as we observe from Equation (4), radar waveforms with more spectral energy at the bandwidth center will reduce the noise spectral density,  $N_{\text{int+n}}(f)$ , due to minimal radar residual values ( $N_{\text{resi}}(f)$ ), thereby maximizing the data rate.

479 Conversely, selecting a larger value for the threshold point  
 480 implies there is more ambiguity in the radar waveform auto-  
 481 correlation function (higher side-lobes), which occurs for radar  
 482 waveforms with more energy at frequencies closer to the edges  
 483 of the bandwidth allocation. Such waveforms also have larger  
 484 RMS bandwidth values and a better estimation performance.  
 485 Finally, radar waveforms with more spectral energy at the  
 486 bandwidth edges have larger  $N_{\text{resi}}(f)$  values and consequently,  
 487 larger  $N_{\text{int+n}}(f)$  values which degrade the communications  
 488 data rate.

489 Thus, we see that selecting a low radar SNR threshold point  
 490 increases the communications performance and decreases the  
 491 radar performance but also results in a radar waveform with  
 492 low side-lobes in the autocorrelation. Similarly, selecting a  
 493 high threshold point increases the radar performance and  
 494 decreases the communications performance but also results  
 495 in a radar waveform with large autocorrelation side-lobes.  
 496 The objective is to select a threshold point that optimizes the  
 497 spectral shape of the radar waveform such that the perfor-  
 498 mance with respect to radar and communications is jointly  
 499 maximized.

500 The results from the numerical study of the above optimiza-  
 501 tion problem are discussed in Section V.

## 502 V. SIMULATION RESULTS

503 In this section, we present an example of the waveform  
 504 design technique discussed in this paper, the minimum estima-  
 505 tion error variance method, for an example parameter set. The  
 506 parameters used in the example are shown in Table II. Addi-  
 507 tionally, a performance comparison of the minimum estimation  
 508 error variance method with the previously derived spectral  
 509 mask shaping method is also provided. We also study the  
 510 effect of the order of the non-linear chirp phase on joint radar-  
 511 communications performance. In order to better solve the  
 512 non-convex optimization problem described in Section IV-B,  
 513 all the results presented below were obtained by solving the  
 514 optimization problem in Equation (21) using *fmincon* [45] for  
 515 100 Monte-Carlo runs with randomized initial solutions and  
 selecting the solution with the highest objective value.

TABLE II  
PARAMETERS FOR WAVEFORM DESIGN METHODS

Parameter	Value
Bandwidth ( $B$ )	5 MHz
Center Frequency	3 GHz
Effective Temperature ( $T_{\text{temp}}$ )	1000 K
Communications Range	10 km
Communications Power ( $P_{\text{com}}$ )	0.3 W
Communications Antenna Gain	0 dBi
Communications Receiver Side-lobe Gain	10 dBi
Radar Target Range	200 km
Radar Antenna Gain	30 dBi
Target Cross Section	10 m <sup>2</sup>
Target Process Standard Deviation ( $\sigma_{\tau, \text{proc}}$ )	100 m
Time-Bandwidth Product ( $TB$ )	128
Radar Duty Factor ( $\delta$ )	0.01
Threshold Point Constraint ( $\delta_{\text{constraint}}$ )	1 + 0.01

516

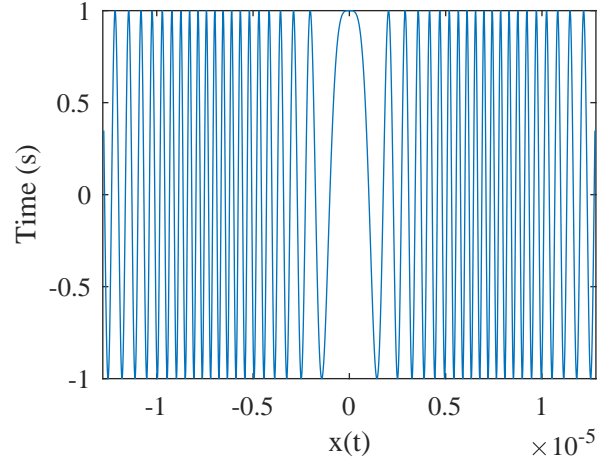


Fig. 6. Real valued amplitude of waveform vs. time (s). We see that the radar waveform has a chip shape similar to a non-linear chirp in the time domain. The constant modulus nature of the radar waveform is also clearly evident.

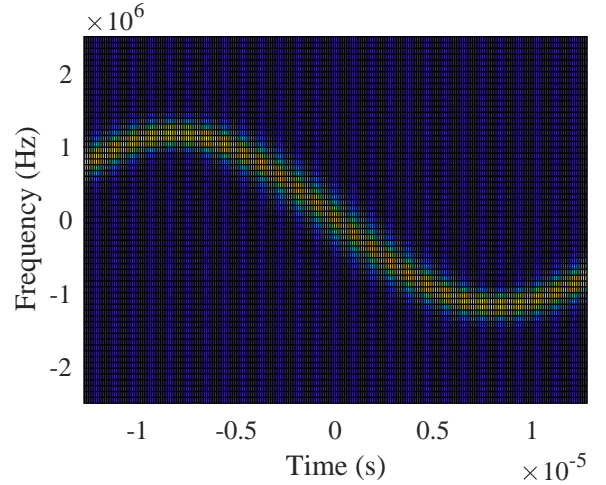


Fig. 7. Short-time Fourier transform spectrogram vs. time (s) and frequency (Hz). We observe that the optimal radar waveform has a non-linear time-frequency representation and is similar to a sum of polynomials.

### 517 A. Minimum Estimation Error Variance Method Optimal 518 Waveform Shape

519 Here we present an example of a joint radar-  
 520 communications optimal radar waveform designed by  
 521 the minimum estimation error variance method. Figures 6  
 522 and 7 show time domain and time-frequency representations  
 523 of the non-linear chirp waveform with polynomial phase  
 524 shown in Equation (13) for the number of polynomial phase  
 525 coefficients,  $N = 6$  and a threshold SNR value of 0dB.  
 526 Figure 6 shows the real valued amplitude of the waveform  
 527 as a function of time. We see that the radar waveform has a  
 528 chip shape similar to a non-linear chirp in the time domain.  
 529 The constant modulus nature of the radar waveform is also  
 530 apparent from the figure. Figure 7 shows the short-time  
 531 Fourier transform spectrogram as a function of time and  
 532 frequency. From this figure, we observe that the optimal radar  
 533 waveform has a non-linear time-frequency representation and  
 534 is similar to a sum of polynomials.



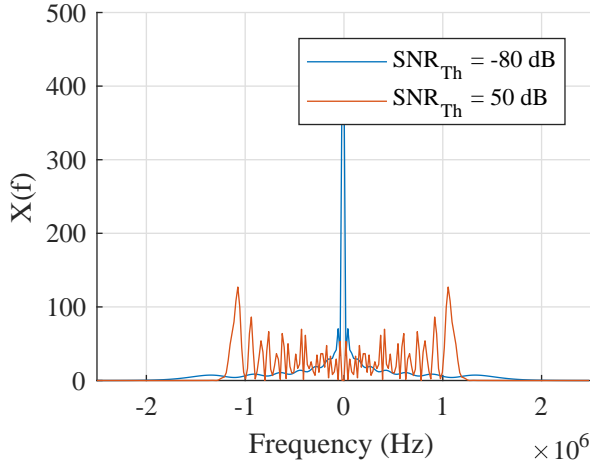


Fig. 8. The minimum estimation error variance optimized radar waveform spectrum for different threshold SNR values. The radar waveform optimization was done for  $N = 6$ . We see the optimal radar spectrum has more spectral energy at the edges of the bandwidth for high threshold SNR values and has more spectral energy closer to the center for low threshold SNR values.

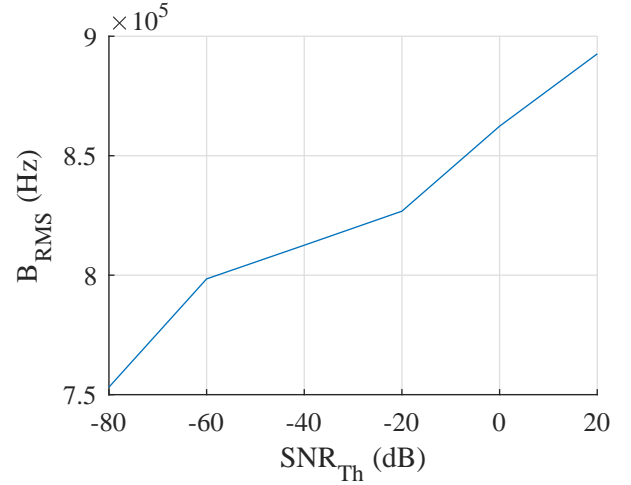


Fig. 9. RMS bandwidth of the optimized radar waveform vs. SNR. As expected, the optimal RMS bandwidth increases as we increase the threshold SNR. From Equation (11), we see that the optimal RMS bandwidth increasing as the threshold SNR increases will thereby reduce the CRLB. As a result, we see that the estimation performance increases with SNR.

### B. Impact of Threshold SNR

We now discuss the numerical results from implementing the minimum estimation error variance method in Section IV-B. First, we highlight the impact of the threshold SNR value on the shape of the radar spectrum. We consider two threshold SNR values of -80dB and 50dB and we choose  $N = 6$  in Equation (13), i.e.,  $x(t) = e^{i\pi(\sum_{m=1}^6 p_m t^{2m})}$ . The minimum estimation error variance optimized radar waveform spectrum for this set of parameters is shown in Figure 8. From Figure 8, we see the optimal radar spectrum has more spectral energy at the edges of the bandwidth for high threshold SNR values and has more spectral energy closer to the center for low threshold SNR values, as we stated in Section IV-C.

We also study the impact of the threshold SNR (or radar SNR) on the system performance. For the purpose of this study, we choose  $N = 6$ . For different values of SNR, we optimize the shape of the waveform, i.e., optimize the coefficients  $\bar{p} = (p_1, \dots, p_6)$ , to minimize the CRLB achieved with the waveform. We also impose the constraint  $\sigma_{est}^2 / \sigma_{CRLB}^2 \leq \delta_{constraint}$ , which ensures that for the given SNR, our feasible solution set include only waveforms whose threshold SNR is less than or equal to the given SNR (as discussed in Section IV-B).  $\delta_{constraint}$  is tuned so that the ratio between the estimation error variance (which characterizes estimation performance in this paper) and the CRLB remains close to 1. For this simulation, we consider a  $\delta_{constraint}$  value of  $1 + \epsilon$ , where  $\epsilon$  introduces some flexibility to the constraint and typically has a value of 0.01.

Figure 9 shows the RMS bandwidth values achieved with each optimized waveform for various values of threshold SNR. As expected, the optimal RMS bandwidth increases as we increase the threshold SNR. From Equation (11) and Section IV-C, we see that the optimal RMS bandwidth increasing as the threshold SNR increases will thereby reduce the CRLB as stated in Section IV-C.

Figure 10 shows the autocorrelation function achieved with each optimized waveform for various values of threshold SNR.

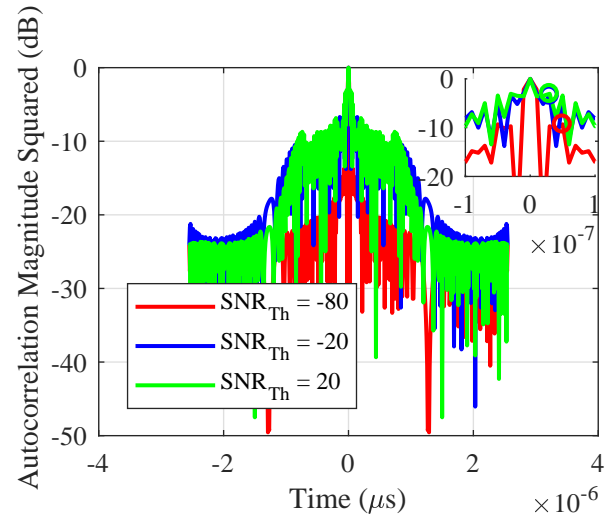


Fig. 10. Autocorrelation function of the optimized radar waveform vs. SNR. As expected, the peak side-lobe of the autocorrelation function increases as we increase the threshold SNR. This trend is observed because a higher threshold SNR implies the optimal waveform has more ambiguity which translates into higher peak autocorrelation side-lobes.

For SNR values -80dB, -20dB and 20dB, we observed that the peak side-lobes in all three cases occur at  $\pm 0.2 - 0.5 \mu s$  and have values of -10dB, -7dB, and -6dB respectively. As expected, the peak side-lobe of the autocorrelation function increases as we increase the threshold SNR. As mentioned in Section IV-C, a higher threshold SNR implies the optimal waveform has more ambiguity which translates into higher peak autocorrelation side-lobes.

Now, for each threshold SNR value we considered and the optimal waveform shape parameters  $p_1, p_2, p_3, p_4, p_5, p_6$  we obtained above, we evaluate the radar estimation rate bound in Equation (8) and the spectral water-filling SIC data rate in Equation (7) corresponding to each of these waveforms.

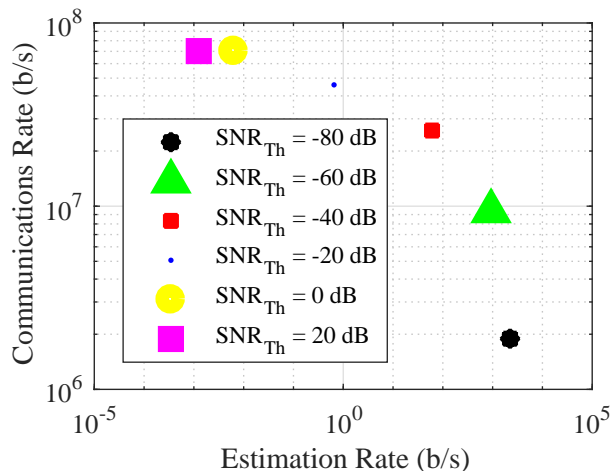


Fig. 11. Estimation and data rates vs. threshold SNR. Clearly, we see the performance of the system improve with respect to the estimation rate and degrade with respect to the spectral water-filling SIC data rate as we increase the threshold SNR.

585 Figure 11 shows the plot of estimation rate and the data rate  
 586 against the threshold SNR value. Clearly, according to the  
 587 figure, the performance of the system improves with respect  
 588 to the estimation rate as we increase the threshold SNR,  
 589 which is expected as the minimum achievable CRLB decreases  
 590 with threshold SNR, and the estimation rate increases with  
 591 decreasing CRLB according to Equation (8) and Equation (9).  
 592 However, we observe that the spectral water-filling SIC data  
 593 rate reduces as the threshold SNR increases. This trend occurs  
 594 because, as we stated in Section IV-C, as the threshold  
 595 SNR increases, the noise spectral density,  $N_{\text{int+n}}(f)$  achieves  
 596 higher values due to larger radar residual values, which reduces  
 597 the spectral water-filling SIC data rate.

### 598 C. Impact of Order of Chirp Phase

599 We first investigate the relationship between the autocorrela-  
 600 tion peak side-lobe levels and the order of the non-linear chirp  
 601 waveform's phase,  $N$ . Figure 12 shows the autocorrelation  
 602 function for  $N = 2$  and  $N = 8$  at a threshold SNR value  
 603 of 0dB. We clearly see that the autocorrelation peak side-  
 604 lobes decrease as  $N$  increases, which causes the estimation  
 605 performance to improve overall as  $N$  increases.

606 As the shape of the waveform explicitly depends on the  
 607 coefficients  $p_1, \dots, p_N$  in Equation (21), we now study the  
 608 effect of the number of coefficients,  $N$ , on both the estimation  
 609 and the data rates. For this study, we choose a threshold SNR  
 610 value of 0dB and vary  $N$  from 1 to 8. For each  $N$  and  
 611 threshold SNR value, we solve Equation (21) and evaluate  
 612 the estimation rate from Equation (8) and spectral water-filling  
 613 SIC data rate from Equation (7). Figure 13 shows plots of these  
 614 rates against  $N$ . From Figure 13, we see that as  $N$  increases,  
 615 the estimation rate increases and the spectral water-filling SIC  
 616 data rate decreases. The improvement in estimation rates as  
 617  $N$  increases is because there are more degrees of freedom  
 618 available to shape the optimal radar waveform spectrum ob-  
 619 tained by solving the optimization problem in Equation (21).  
 620 As a result of these increased degrees of freedom, optimal

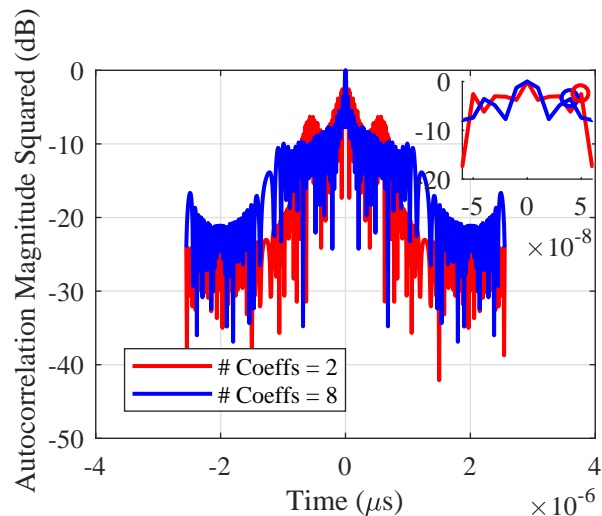


Fig. 12. Autocorrelation function of the optimized radar waveform vs.  $N$ . We clearly see that the autocorrelation peak side-lobes decrease as  $N$  increases, which causes the estimation performance to improve overall as  $N$  increases.

621 radar waveforms are obtained that have better or lower au-  
 622 tocorrelation side-lobe levels (a trend we observed earlier).  
 623 Additionally, increasing  $N$  means increasing the amount of  
 624 energy at higher frequencies for the radar waveform spectrum,  
 625 which results in the  $B_{\text{rms}}$  value increasing, there by improving  
 626 local estimation performance given by Equation (11). This  
 627 increase in local estimation performance, coupled with lower  
 628 autocorrelation side-lobe levels, results in an overall increase  
 629 in the estimation rate as  $N$  increases. Furthermore, the increase  
 630 in the radar waveform's spectral content at higher frequencies,  
 631 due to an increase in  $N$ , means that the noise spectral density,  
 632  $N_{\text{int+n}}(f)$ , achieves higher values due to larger radar residual  
 633 values, which reduces the spectral water-filling SIC data rate.

### 634 D. Performance Comparison of Waveform Design Algorithms

635 Next, we compare the performance of the minimum estima-  
 636 tion error variance method against the spectral mask shaping  
 637 method in [6]. We conduct a Monte Carlo study with 50 runs to  
 638 compare the performance of these methods. For this study, we  
 639 choose the SNR of 7.6dB, and set  $N = 6$ . In each Monte Carlo  
 640 run, we evaluate the estimation rates and the communications  
 641 rates (spectral water-filling SIC data rate for the minimum  
 642 estimation error variance method and the SIC data rate for  
 643 the spectral mask shaping method) from the two methods.  
 644 Table III shows the average of estimation rates ( $R_{\text{est}}$ ) and  
 645 communications rates ( $R_{\text{com}}$ ) from the Monte-Carlo study.

646 From Table III, we clearly observe that the minimum esti-  
 647 mation error variance method outperforms the spectral-mask  
 648 shaping method in terms of estimation rate and communica-  
 649 tions rate. Furthermore, a significant increase in the achieved  
 650 communications rate highlights the impact of the continuous  
 651 water-filling algorithm. Thus, we see the explicit advantage  
 652 of the proposed method over the method in [6] in that the  
 653 minimum estimation error variance method proposed in this  
 654 paper designs radar waveforms that are constant modulus and

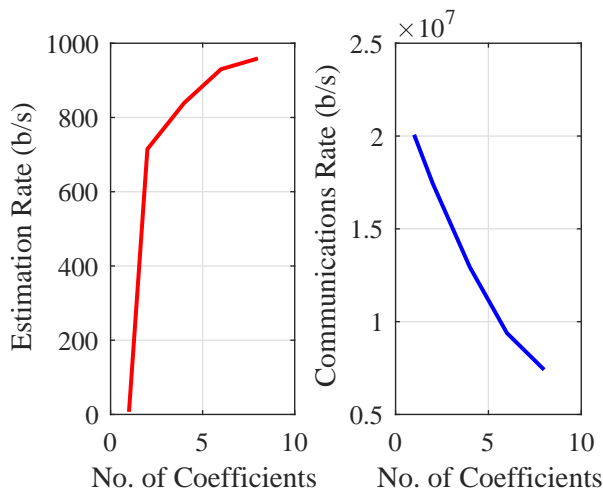


Fig. 13. Estimation and data rates vs.  $N$ . We see that as  $N$  increases, the estimation rate increases and the spectral water-filling SIC data rate decreases. The improvement in estimation rates as  $N$  increases is because there are more degrees of freedom available to shape the optimal radar waveform spectrum, which results in optimal waveforms that have better or lower autocorrelation side-lobe levels. Additionally, increasing  $N$  means increasing the amount of energy at higher frequencies for the radar waveform spectrum, which improves local estimation performance. Furthermore, the increase in the radar waveform's spectral content at higher frequencies, due to an increase in  $N$ , means that the noise spectral density,  $N_{\text{int+n}}(f)$ , achieves higher values due to larger radar residual values, which reduces the spectral water-filling SIC data rate.

ensures better estimation performance and better communications performance over the spectral shaping method.

TABLE III  
MINIMUM ESTIMATION ERROR VS. SPECTRAL-MASK SHAPING FOR SNR = 7.6dB

Performance metric (average values)	Min. Est. Error	Spectral-Mask Shaping
$R_{\text{est}}$ (b/s)	$1.38 \times 10^3$	$3.05 \times 10^3$
$R_{\text{com}}$ (b/s)	$6.92 \times 10^6$	$1.38 \times 10^4$

## VI. CONCLUSIONS

In this paper, we presented a novel radar waveform design technique that maximizes the performance of a spectrum sharing, joint radar-communications system. The global estimation rate, an extension on the estimation rate that takes into account non-local or global estimation errors, and the data rate are used to measure radar and communications performance respectively. We developed the novel minimum estimation error variance radar waveform design method that selects the phase parameters of a nonlinear chirp radar waveform to maximize radar performance. We also developed the spectral water-filling SIC data rate which is the maximized communications data rate for a joint radar-communications receiver employing SIC. This maximized data rate was obtained by employing the continuous spectral water-filling algorithm which determines the optimal communications power spectral distribution for a given noise spectral density. We presented examples of the minimum estimation error variance radar waveform design method for an example parameter set and also compared

the method's performance against the performance of the previously derived spectral mask shaping method. We saw that the minimum estimation error variance method is able to achieve higher estimation and communications data rate values than the spectral mask shaping method. We also observed that the optimal estimation rate increases for higher radar SNR values whereas the optimal spectral-water-filling SIC data rate decreases for higher radar SNR values. Finally, we observed that the estimation rate increases and the spectral water-filling SIC data rate decreases as the number of coefficients in the phase of the non-linear chirp increases.

## REFERENCES

- [1] B. Paul, A. R. Chiriyath, and D. W. Bliss, "Survey of RF communications and sensing convergence research," *IEEE Access*, vol. 5, no. 1, pp. 252–270, December 2016.
- [2] H. Griffiths, L. Cohen, S. Watts, E. Mokole, C. Baker, M. Wicks, and S. Blunt, "Radar spectrum engineering and management: Technical and regulatory issues," *Proceedings of the IEEE*, vol. 103, no. 1, pp. 85–102, January 2015.
- [3] D. W. Bliss, "Cooperative radar and communications signaling: The estimation and information theory odd couple," in *IEEE Radar Conference*, May 2014, pp. 50–55.
- [4] A. R. Chiriyath, B. Paul, and D. W. Bliss, "Radar-communications convergence: coexistence, cooperation, and co-design," *IEEE Transactions on Cognitive Communications and Networking*, vol. 3, no. 1, pp. 1–12, February 2017.
- [5] A. R. Chiriyath, B. Paul, G. M. Jacyna, and D. W. Bliss, "Inner bounds on performance of radar and communications co-existence," *IEEE Transactions on Signal Processing*, vol. 64, no. 2, pp. 464–474, January 2016.
- [6] B. Paul, A. R. Chiriyath, and D. W. Bliss, "Joint communications and radar performance bounds under continuous waveform optimization: The waveform awakens," in *IEEE Radar Conference*, May 2016, pp. 865–870.
- [7] T. M. Cover and J. A. Thomas, *Elements of Information Theory*, 2nd ed. Hoboken, New Jersey: John Wiley & Sons, 2006.
- [8] B. Paul and D. W. Bliss, "The constant information radar," *Entropy*, vol. 18, no. 9, p. 338, 2016. [Online]. Available: <http://www.mdpi.com/1099-4300/18/9/338>
- [9] A. R. Chiriyath, B. Paul, and D. W. Bliss, "Simultaneous radar detection and communications performance with clutter mitigation," in *IEEE Radar Conference*, May 2017, pp. 279–284.
- [10] C. Sturm and W. Wiesbeck, "Waveform design and signal processing aspects for fusion of wireless communications and radar sensing," *Proceedings of the IEEE*, vol. 99, no. 7, pp. 1236–1259, July 2011.
- [11] A. Turlapaty, Y. Jin, and Y. Xu, "Range and velocity estimation of radar targets by weighted OFDM modulation," in *IEEE Radar Conference*, May 2014, pp. 1358–1362.
- [12] T. Guo and R. Qiu, "OFDM waveform design compromising spectral nulling, side-lobe suppression and range

- 732 resolution,” in *IEEE Radar Conference*, May 2014, pp. 733 1424–1429.
- 734 [13] G. Lellouch, A. Mishra, and M. Inggs, “Impact of the 735 Doppler modulation on the range and Doppler processing 736 in OFDM radar,” in *IEEE Radar Conference*, May 2014, 737 pp. 803–808.
- 738 [14] S. C. Thompson and J. P. Stralka, “Constant envelope 739 OFDM for power-efficient radar and data communica- 740 tions,” in *International Waveform Diversity and Design 741 Conference*, February 2009, pp. 291–295.
- 742 [15] X. Shaojian, C. Bing, and Z. Ping, “Radar- 743 communication integration based on DSSS techniques,” 744 in *8th International Conference on Signal Processing*, 745 vol. 4, November 2006, pp. 1–4.
- 746 [16] Y. Xie, R. Tao, and T. Wang, “Method of waveform 747 design for radar and communication integrated system 748 based on CSS,” in *First International Conference on In- 749 strumentation, Measurement, Computer, Communication 750 and Control*, October 2011, pp. 737–739.
- 751 [17] M. Robertson and E. R. Brown, “Integrated radar and 752 communications based on chirped spread-spectrum tech- 753 niques,” in *2003 IEEE MTT-S International Microwave 754 Symposium Digest*, vol. 1, June 2003, pp. 611–614.
- 755 [18] A. Khawar, A. Abdel-Hadi, and T. C. Clancy, “MIMO 756 radar waveform design for coexistence with cellular 757 systems,” in *IEEE International Symposium on Dynamic 758 Spectrum Access Networks (DYSPAN)*, April 2014, pp. 759 20–26.
- 760 [19] Y. L. Sit and T. Zwick, “MIMO OFDM radar with 761 communication and interference cancellation features,” 762 in *IEEE Radar Conference*, May 2014, pp. 265–268.
- 763 [20] B. Li, A. P. Petropulu, and W. Trappe, “Optimum co- 764 design for spectrum sharing between matrix completion 765 based MIMO radars and a MIMO communication sys- 766 tem,” *IEEE Transactions on Signal Processing*, vol. 64, 767 no. 17, pp. 4562–4575, May 2016.
- 768 [21] Y. Zhang, Q. Li, L. Huang, and J. Song, “Waveform 769 design for joint radar-communication system with multi- 770 user based on MIMO radar,” in *2017 IEEE Radar Con- 771 ference (RadarConf)*, May 2017, pp. 0415–0418.
- 772 [22] A. Aubry, V. Carotenuto, A. De Maio, A. Farina, 773 and L. Pallotta, “Optimization theory-based radar wave- 774 form design for spectrally dense environments,” *IEEE 775 Aerospace and Electronic Systems Magazine*, vol. 31, 776 no. 12, pp. 14–25, December 2016.
- 777 [23] Y. Huang, M. Piezzo, V. Carotenuto, and A. De Maio, 778 “Radar waveform design under similarity, bandwidth 779 priority, and spectral coexistence constraints,” in *2017 780 IEEE Radar Conference (RadarConf)*, May 2017, pp. 781 1142–1147.
- 782 [24] A. Aubry, V. Carotenuto, and A. De Maio, “Radar 783 waveform design with multiple spectral compatibility 784 constraints,” in *2016 IEEE Radar Conference (Radar- 785 Conf)*, May 2016, pp. 1–6.
- 786 [25] J. Qian, M. Lops, L. Zheng, X. Wang, and Z. He, 787 “Joint system design for coexistence of mimo radar and 788 mimo communication,” *IEEE Transactions on Signal 789 Processing*, vol. 66, no. 13, pp. 3504–3519, 2018.
- [26] A. Khawar, A. Abdel-Hadi, and T. C. Clancy, “Spectrum 790 sharing between S-band radar and LTE cellular system: 791 A spatial approach,” in *IEEE International Symposium 792 on Dynamic Spectrum Access Networks (DYSPAN)*, April 793 2014, pp. 7–14. 794
- [27] S. Sodagari, A. Khawar, T. C. Clancy, and R. McGwier, 795 “A projection based approach for radar and telecommu- 796 nication systems coexistence,” in *IEEE Global Commu- 797 nications Conference (GLOBECOM)*, Decemeber 2012, 798 pp. 5010–5014. 799
- [28] H. Shajaiah, A. Abdelhadi, and C. Clancy, “Spectrum 800 sharing approach between radar and communication sys- 801 tems and its impact on radars detectable target param- 802 eters,” in *IEEE 81st Vehicular Technology Conference 803 (VTC Spring)*, May 2015, pp. 1–6. 804
- [29] W. Zhang, S. Vedantam, and U. Mitra, “Joint transmis- 805 sion and state estimation: A constrained channel coding 806 approach,” *IEEE Transactions on Information Theory*, 807 vol. 57, no. 10, pp. 7084–7095, October 2011. 808
- [30] P. Stinco, M. Greco, F. Gini, and B. Himed, “Channel 809 parameters estimation for cognitive radar systems,” in 810 *2014 4th International Workshop on Cognitive Informa- 811 tion Processing (CIP)*, May 2014, pp. 1–6. 812
- [31] A. Pezeshki, A. R. Calderbank, W. Moran, and S. D. 813 Howard, “Doppler resilient Golay complementary wave- 814 forms,” *IEEE Transactions on Information Theory*, 815 vol. 54, no. 9, pp. 4254–4266, September 2008. 816
- [32] B. Li and A. Petropulu, “MIMO radar and communica- 817 tion spectrum sharing with clutter mitigation,” in *2016 818 IEEE Radar Conference (RadarConf)*, May 2016, pp. 1– 819 6. 820
- [33] D. W. Bliss and S. Govindasamy, *Adaptive Wireless 821 Communications: MIMO Channels and Networks*. New 822 York, New York: Cambridge University Press, 2013. 823
- [34] A. Sabharwal, P. Schniter, D. Guo, D. W. Bliss, S. Ran- 824 garajan, and R. Wichman, “In-band full-duplex wireless: 825 Challenges and opportunities,” *IEEE Journal on Selected 826 Areas in Communications*, vol. 32, no. 9, pp. 1637–1652, 827 September 2014. 828
- [35] D. W. Bliss, P. A. Parker, and A. R. Margetts, “Simulta- 829 neous transmission and reception for improved wireless 830 network performance,” in *2007 IEEE/SP 14th Workshop 831 on Statistical Signal Processing*, Aug 2007, pp. 478–482. 832
- [36] A. R. Chiriyath, B. Paul, and D. W. Bliss, “Joint radar- 833 communications information bounds with clutter: The 834 phase noise menace,” in *IEEE Radar Conference*, May 835 2016, pp. 690–695. 836
- [37] R. G. Gallager, *Information Theory and Reliable Com- 837 munication*, 2nd ed. Hoboken, New Jersey: John Wiley 838 & Sons, 1968. 839
- [38] S. M. Kay, *Fundamentals of Statistical Signal Process- 840 ing: Estimation Theory*, 1st ed. Upper Saddle River, NJ, 841 USA: Prentice-Hall, Inc., 1993. 842
- [39] C. D. Richmond, “Mean-squared error and threshold 843 SNR prediction of maximum-likelihood signal parameter 844 estimation with estimated colored noise covariances,” 845 *IEEE Transactions on Information Theory*, vol. 52, no. 5, 846 pp. 2146–2164, May 2006. 847

- 848 [40] H. Van Trees, *Detection, Estimation, and Modulation*  
849 *Theory: Part 1*, 1st ed. Hoboken, New Jersey: John  
850 Wiley & Sons, 2004.
- 851 [41] M. A. Richards, *Principles of Modern Radar: Basic*  
852 *Principles*, J. A. Sheer and W. A. Holm, Eds. Raleigh,  
853 North Carolina: SciTech Publishing, 2010.
- 854 [42] B. Paul and D. W. Bliss, "Extending joint radar-  
855 communications bounds for FMCW radar with Doppler  
856 estimation," in *IEEE Radar Conference*, May 2015, pp.  
857 89–94.
- 858 [43] M. A. Richards, *Fundamentals of Radar Signal Process-*  
859 *ing*, 2nd ed. Raleigh, North Carolina: McGraw-Hill  
860 Professional, 2013.
- 861 [44] S. Das and P. N. Suganthan, "Differential evolution: A  
862 survey of the state-of-the-art," *IEEE Transactions on*  
863 *Evolutionary Computation*, vol. 15, no. 1, pp. 4–31,  
864 February 2011.
- 865 [45] MATLAB's *fmincon*. [Online]. Available:  
866 [https://www.mathworks.com/help/optim/ug/fmincon.](https://www.mathworks.com/help/optim/ug/fmincon.html?requestedDomain=www.mathworks.com)  
867 [html?requestedDomain=www.mathworks.com](https://www.mathworks.com/help/optim/ug/fmincon.html?requestedDomain=www.mathworks.com)